Proceedings of the 18th International Conference on Nuclear Engineering
ICONE18
May 17-21, 2010, Xi`an, China

ICONE18-29659

NUMERICAL SIMULATION OF CAVITATION FOR COMPARISON OF SODIUM AND WATER FLOWS

Teddy Ardiansyah*
Department of Nuclear Engineering
Tokyo Institute of Technology
2-12-1-N1-18, O-okayama, Meguro-ku,
Tokyo, 152-8550, Japan
+81-3-5734-2957, +81-3-5734-2959(fax)
ardiansyah.t.aa@m.titech.ac.jp

Minoru Takahashi
Research Laboratory for Nuclear Reactors
Tokyo Institute of Technology
2-12-1-N1-18, O-okayama, Meguro-ku,
Tokyo, 152-8550, Japan
+81-3-5734-2957, +81-3-5734-2959(fax)
mtakahas@nr.titech.ac.jp

Yoshio Yoshizawa
Research Laboratory for Nuclear Reactors
Tokyo Institute of Technology
2-12-1-N1-18, O-okayama, Meguro-ku,
Tokyo, 152-8550, Japan
+81-3-5734-2963, +81-3-5734-2959(fax)
yyoshiza@nr.titech.ac.jp

Masamichi Nakagawa
Department of Mechanical Sciences and Engineering
Tokyo Institute of Technology
2-12-1-N1-18, O-okayama, Meguro-ku,
Tokyo, 152-8550, Japan
nakagawa@mech.titech.ac.jp

Makoto Asaba
Sukegawa Electric Co., Ltd.
3-19-5, Namekawahontyo, Hitachi,
Ibaraki, 317-0051, Japan
asaba@net-sukegawa.com

Kuniaki Miura
Sukegawa Electric Co., Ltd.
3-19-5, Namekawahontyo, Hitachi,
Ibaraki, 317-0051, Japan
miura@net-sukegawa.com

ABSTRACT

In this paper, numerical simulation of cavitation for water and sodium flows were performed by using CFD code package FLUENT and the results were compared with the experiments. The geometry of the grid for numerical calculation was a venturi with ID and OD of 6.5 and 21 mm, respectively. The numerical simulations showed that the onset cavitation conditions were affected significantly by the non-condensable gas content in the liquid. Comparing with the experimental results, the non-condensable gas contents that gave close predictions of onset cavitation conditions with the experiments were larger in water than in liquid sodium because of the different solubility property of air and argon gas. Parametrical analysis showed that the void fraction distributions for water and liquid sodium did not show large differences in case of the same cavitation coefficient and non-condensable gas contents.

1. INTRODUCTION

Cavitation is the formation of bubbles in flowing liquid due to reduction of pressure below its saturation pressure in accelerated high velocity liquid. In water flow system such as pumps and orifices, cavitation has been known to cause severe and undesirable problems such as vibrations, erosion and noise. This phenomenon has been intensively investigated by several authors in the past such as by Testud, et al [1], Koivula [2] and Courbiere [3]. It is potentially possible that cavitation occurs not only in the water flow system but also in liquid metal coolant of the future nuclear reactor such as sodium-cooled fast reactor (SFR) depending on fluid-dynamic design. In the

development of economic SFR, reactor vessel and flow components are made compact, which leads to fast flow of coolant. This fast flow of coolant might cause cavitation if the local static pressure falls below its saturation pressure.

One of the key issues in fluid-dynamic design of the SFRs is inhibition of cavitation and/or its influences. The influences are classified into fluid-dynamic, mechanical, and core neutronics performances as follows: the occurrence of cavitation affects fluid-dynamic performances of flow regulating mechanisms in inner structure of reactor vessel; the collapse of cavitation bubbles produces shock waves that damage the edges of orifices, which changes flow rate distribution in core; the shock waves also damage structural material and piping walls; vibrations due to cavitation cause metal fatigue of piping systems; and the entry of cavitation bubbles into core causes instability of core reactivity. According to Kale and Rajan [4], the damage caused by the cavitation in liquid metal is 1.5-2 times more severed than in water and the formation of vapor cavities in fuel element passages are not acceptable due to the resulting overheating of fuel clad and its implications.

Most of the research on cavitation phenomena in the flowing liquid sodium utilizes water to substitute the highly reactive sodium. This substitution could raise a question whether the results could be comparable or not. Therefore in order to make clear the phenomena, this present study was conducted to investigate numerically cavitation phenomena in water and liquid sodium and compare the results with each other. Parametrical analysis is also included in the calculations as well as comparison with the experimental results obtained by the authors [5].

2. MIXTURE MODEL THEORY

The model used to simulate multiphase flow is the multiphase mixture model. It is a simplified multiphase model where gas bubbles and liquid flow at the same velocity as local equilibrium over short spatial length scales. The mixture model solves the continuity, momentum, and energy equations for the two-phase mixture as well as the volume fraction equation for the secondary phases.

- Continuity equation for the two-phase mixture

$$\frac{\partial}{\partial t}\left(\rho_m\right)+\nabla.\left(\rho_m\vec{\upsilon}_m\right)=0 \tag{1}$$

- Momentum equation for the two-phase mixture

$$\frac{\partial}{\partial t}\left(\rho_m\vec{\upsilon}_m\right)+\nabla.\left(\rho_m\vec{\upsilon}_m\vec{\upsilon}_m\right)=-\nabla p + \nabla.\left[\mu_m\left(\nabla\vec{\upsilon}_m+\nabla\vec{\upsilon}_m^{T}\right)\right]+\rho_m\vec{g}+\vec{F} + \nabla.\left(\sum_{k=1}^{n}\alpha_k\rho_k\vec{\upsilon}_{dr,k}\vec{\upsilon}_{dr,k}\right) \tag{2}$$

- Energy equation for the two-phase mixture

$$\frac{\partial}{\partial t}\sum_{k=1}^{n}\left(\alpha_k\rho_k E_k\right)+\nabla.\sum_{k=1}^{n}\left(\alpha_k\vec{\upsilon}_k\left(\rho_k E_k+p\right)\right) = \nabla.\left(k_{eff}\nabla T\right)+S_E \tag{3}$$

and

$$E_k = h_k-\frac{p}{\rho_k}+\frac{\upsilon_k^2}{2} \tag{4}$$

for a compressible phase. $E_k = h_k$ for an incompressible phase.

- Volume fraction equation for secondary phase, p

$$\frac{\partial}{\partial t}\left(\alpha_p\rho_p\right)+\nabla.\left(\alpha_p\rho_p\overrightarrow{\upsilon_m}\right)=-\nabla.\left(\alpha_p\rho_p\vec{\upsilon}_{dr,p}\right) + \sum_{q=1}^{n}\left(\dot{m}_{qp}-\dot{m}_{pq}\right) \tag{5}$$

3. CAVITATION MODEL

The cavitation model used in the numerical calculation is the full cavitation model based on the work by Singhal, *et al.* [6]. This model is embedded in the CFD code FLUENT version 6.3.26 as the basic cavitation model. The basic cavitation model in FLUENT has the following assumptions [7]:

- the system under investigation involves two phases (liquid and its vapor) and a certain fraction of modeled non-condensable gases.
- both bubble formation (evaporation) and collapse (condensation) are taken into account in the model.
- the mass fraction of non-condensable gas is known in advance.

3.1. Vapor mass fraction and transport

The governing equation for the transport of vapor mass fraction, f, is given by:

$$\frac{\partial}{\partial t}\left(\rho_m f\right)+\nabla\left(\rho_m\overrightarrow{v_v}f\right)=\nabla\left(\gamma\nabla f\right)+R_e-R_c \tag{6}$$

where R_e and R_c are derived from the Rayleigh-Plesset equations and limiting bubble size considerations (interface surface area per unit volume) [6].

when $p < p_{sat}$

$$R_e = C_e\frac{V_{ch}}{\sigma}\rho_l\rho_v\sqrt{\frac{2\left(p_{sat}-p\right)}{3\rho_l}}\left(1-f\right) \tag{7}$$

when $p < p_{sat}$

$$R_c = C_c\frac{V_{ch}}{\sigma}\rho_l\rho_v\sqrt{\frac{2\left(p_{sat}-p\right)}{3\rho_l}}f \tag{8}$$

C_e and C_c are empirical constants with default value of 0.02 and 0.01, respectively. V_{ch} is the characteristic velocity which is approximated by the local turbulence intensity, i.e. $V_{ch} = \sqrt{k}$.

3.2. Turbulence induced pressure fluctuations

The effect of turbulence on cavitating flow is included in the FLUENT's cavitation model and the equation for p_{sat} is therefore changed to the form

$$p_v = 0.5\left(p_{sat} + p_{turb}\right) \tag{9}$$

where

$$p_{turb} = 0.39\rho k \tag{10}$$

3.3. Effect of non-condensable gases, β

The working fluid in the FLUENT's cavitation model is assumed to be a mixture of the liquid phase and the gaseous phase, with the gaseous phase comprising of the liquid vapor and the non-condensable gases. With the effect of non-condensable gases, the density of the mixture, ρ_m , is calculated as

$$\rho_m = \alpha_\upsilon \rho_\upsilon + \alpha_g \rho_g + \left(1 - \alpha_\upsilon - \alpha_g\right)\rho_l \tag{11}$$

The relationship between the mass fraction, f_i , and the volume fraction, α_i is

$$\alpha_i = f_i \frac{\rho}{\rho_i} \tag{12}$$

3.4. Phase change rates

The final form of the phase change rates (Eq. 6 an 7) after accounting for the effects of turbulence and non-condensable gases are

when $p < p_\upsilon$

$$R_e = C_e \frac{\sqrt{k}}{\sigma} \rho_l \rho_v \sqrt{\frac{2\left(p_\upsilon - p\right)}{3\rho_l}} \left(1 - f_\upsilon - f_g\right) \tag{13}$$

when $p < p_\upsilon$

$$R_c = C_c \frac{\sqrt{k}}{\sigma} \rho_l \rho_v \sqrt{\frac{2\left(p_\upsilon - p\right)}{3\rho_l}} f_\upsilon \tag{14}$$

4. TEST SECTION GEOMETRY

The simulated test section for numerical calculation is based on the cavitation experiments conducted by the authors in water and liquid sodium. The geometry of the venturi part of the test section for both sodium and water cavitation experiments is similar and can be seen in Fig. 1. The inner diameter (D1) and outer diameter (D0) is 6.5 mm and 21 mm, respectively.

Figure 4 shows the grid for the numerical solution. It consists of 11440 quadrilateral cells, axisymmetric. The results of the grid sensitivity dependency on the numerical solution are shown in Fig. 5. It shows that the numerical result of 11440 cells have no significant difference with a test section comprising of 45760 cells.

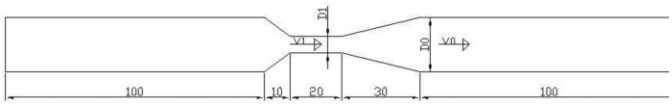

Figure 1. Venturi test section for cavitation experiment (length is in mm).

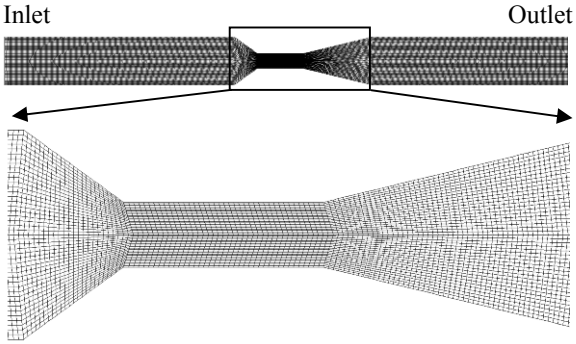

Figure 2. Grid for numerical solution.

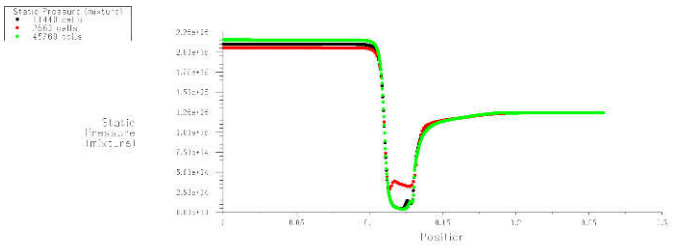

Figure 3. Grid sensitivity check.

5. CAVITATION COEFFICIENT *K*

The cavitation coefficient *K* is derived from the Bernoulli`s equation for incompressible flow.

$$P_1 + \frac{\rho}{2} V_1^2 = P_0 + \frac{\rho}{2} V_0^2 \tag{15}$$

If P_1 is close to the saturation pressure P_υ of the liquid, then the cavitation coefficient *K* can be expressed as

$$K = \frac{P_0 - P_v}{\frac{\rho}{2}\left(V_1^2 - V_0^2\right)} \tag{16}$$

and for $V_1 >> V_0$

$$K \approx \frac{P_0 - P_v}{\frac{\rho}{2} V_1^2} \tag{17}$$

According to the theory, cavitation starts to occur when cavitation coefficient K is nearly equal to unity.

6. BOUNDARY CONDITIONS, LIQUID DENSITY AND VAPOR PRESSURE

The boundary conditions for the numerical calculation is fixed velocity at the inlet and fixed pressure at the outlet. These values are obtained from the experiments conducted by the authors using water and liquid sodium. The details of the sodium loop are described in Ref. [5]. The water loop for cavitation experiment was constructed at Research Laboratory for Nuclear Reactors (RLNR), Tokyo Institute of Technology as shown in the figure below.

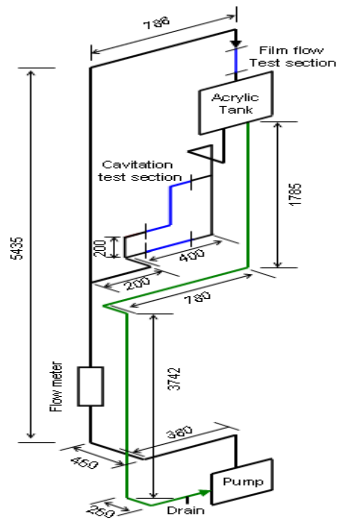

Figure 4. Water loop test apparatus.

The loop itself consists of four main parts, i.e. the pump, the flow meter, the tank made from acrylic resin and the test section. The pump is a canned motor pump supplied by Teikoku Electric MFG. Co., Ltd. This pump is connected to an inverter to control the rotation speed of the pump. The flow meter is an orifice type and used to measure the flow rate of water based on pressure difference between the upstream and downstream of the flow. This flow meter is connected with a differential pressure transducer whose output signal is proportional to the pressure difference. At the top of the loop, there is the large tank to contain water and circulate it during experiment. The venturi test section is mounted below the tank. Cavitation experiment in water loop uses tap water that is filtered. The temperature of the water is ambient temperature. Before experiments, the loop is evacuated by using a vacuum pump to a certain value of pressure (stagnant pressure). The rpm speed of the canned motor pump is increased gradually until cavitation occurs at the venturi test section and the data are recorded by using a computer.

The liquid density of water in this experiment is 1000 kg/m^3, while for sodium the liquid density is calculated as Ref. [8]

$$\rho = 219 + 275.32\left(1 - \frac{T(K)}{2503.7}\right) + 511.58\left(1 - \frac{T(K)}{2503.7}\right)^{0.5} \tag{18}$$

The vapor pressure for water and sodium is calculated by the following equations,
for water (Antoine equation)

$$\log P(torr) = 8.07131 - \frac{1730.63}{233.426 + T(K)} \tag{19}$$

and for sodium [8]

$$\ln P(MPa) = 11.9463 - \frac{12633.73}{T(K)} - 0.4672 \ln T(K) \tag{20}$$

7. RESULTS AND DISCUSSIONS

Cavitation occurrences in numerical calculation are judged from the void fraction distribution over the test section's length. Figure 5a shows the result of void fraction distributions for water. The inlet and outlet of the venturi is at 110 mm and 130 mm, respectively. The figure indicates a sharp increase of the void fraction for cavitation coefficient, K, equals to 1.08 and 0.98. At these values, cavitation starts to occur because there is a sudden change of the void fraction distribution at the venturi part. This increase is caused by the formation of cavity bubbles at the venturi due to a large decrease of static pressure below the vapor pressure of the liquid as shown in Fig. 5b by assuming that the non-condensable gas content is 15 ppm which is a typical value for tap water. For the present experiments, we did not measure the solubility of air and argon gas in water and liquid sodium, respectively.

Numerical calculation results of onset cavitation conditions in water and liquid sodium compared with the experiments for different value of non-condensable gases (beta) are shown in Figs. 6 and 7. In water, the non-condensable gas is air while in liquid sodium is argon gas. For both cases, the change of the non-condensable gas has significant effects on the onset conditions of cavitation. The onset conditions of cavitation increase with the increase of non-condensable gases because their existences in the fluid could act as nucleation sites for the

growth of cavity bubbles. Bistafa [9] in his experiment stated that the gas content is very influential in the inception mechanism of cavitation. He showed that gaseous cavitation due to diffusion of air into the nuclei is easy to occur for flow with higher air concentration than lower air concentration. The number of bubbles also increases for flow with higher air concentration than for lower one.

From the figures, for water with non-condensable gas content of 45 ppm, the results are close to the experimental data. While in sodium, the content of non-condensable gas that gives the results close with the experimental data is 1 ppm. The difference of non-condensable gas content might be caused by the different solubility of air and argon gas in water and liquid sodium. In water, air is easily dissolved while in liquid sodium, argon gas is not easily dissolved. For instance in equilibrium condition, the solubility of argon gas at 400°C calculated by Veleckis correlation [10] and the solubility of water at 10.8°C calculated based on Ref. [11] are 2.83 ppm and 22.18 ppm, respectively. But the values of non-condensable gases in the numerical calculations that gives the results close to the experimental data are much higher than the calculated values at equilibrium conditions. These conditions might be caused by a lot of factors such as liquid impurities, trapped gas pockets or entrainment of gas into the flowing liquids which could also act as nucleation sites for the growing of cavitation bubbles inside the venturi test section.

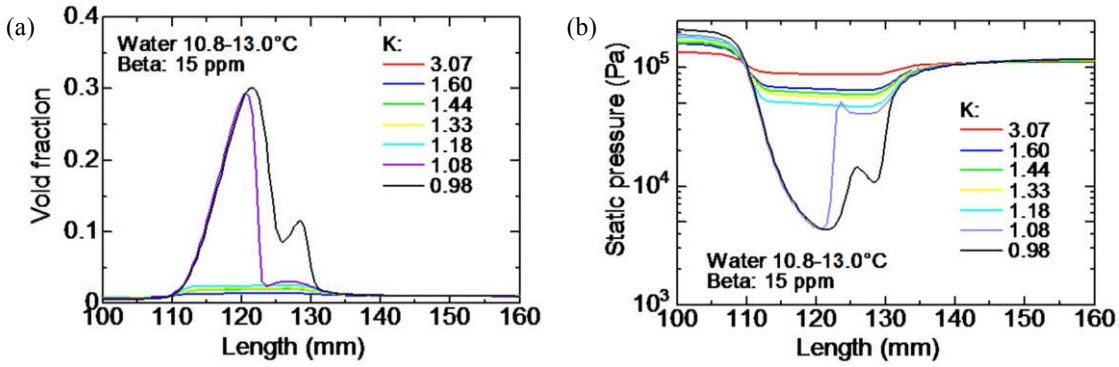

Figure 5. Calculation results of a) Void fraction and, b) Static pressure at central axis of the test section.

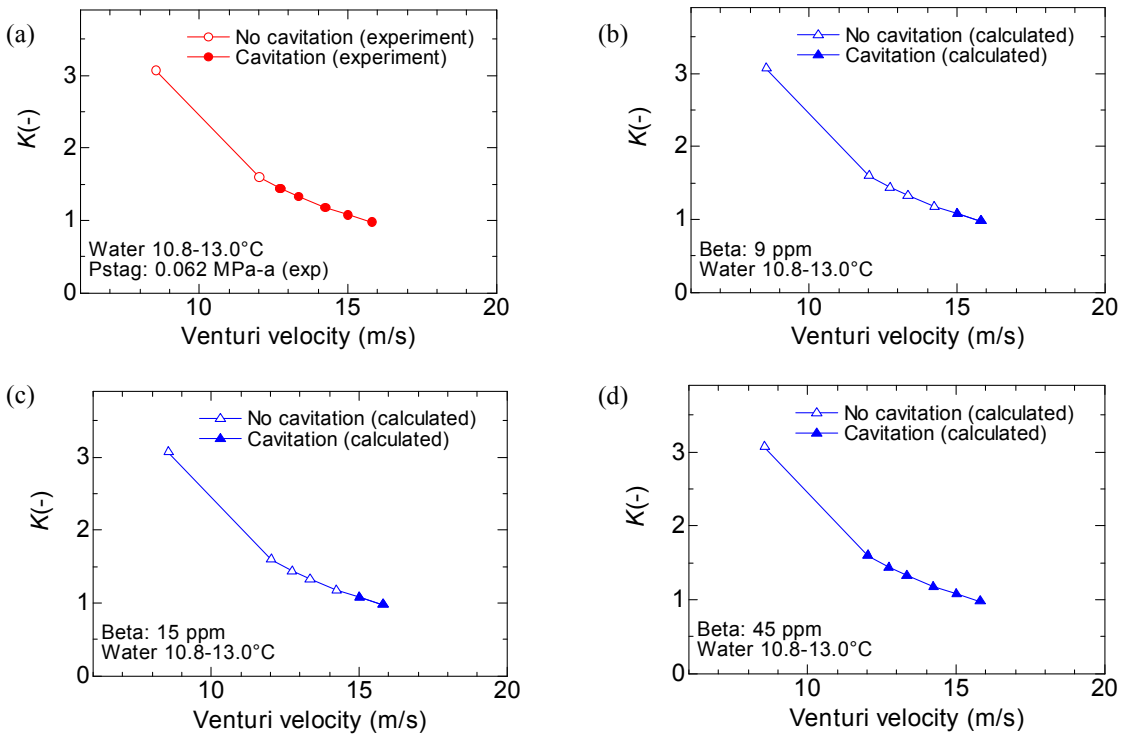

Figure 6. Comparison of onset cavitation condition in water (flow rate: 17.02~31.47 l/min; K: 3.07~0.98; P_{ds}: 0.114~0.124 MPa-a).

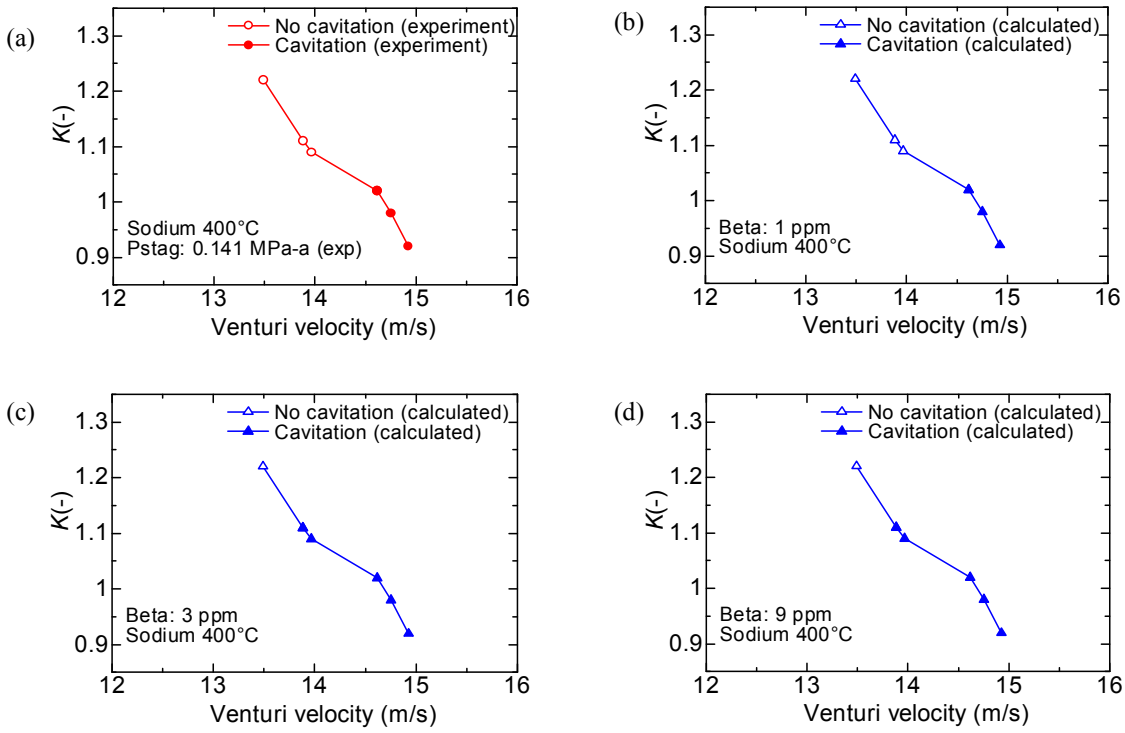

Figure 7. Comparison of onset cavitation condition in sodium (flow rate: 26.86~29.72 l/min; K: 1.22~0.93; P_{ds}: 0.094~0.087 MPa-a).

Figures 8 and 9 show the contours of void fraction for water and liquid sodium. The contours show the formations of voids (cavity bubbles) at the throat of the venturi inlet. The high void fractions (cavity bubbles) are caused by the high turbulent intensity and large pressure drop when the liquid (water and sodium) flowing through the throat of the venturi region. Because of the increase of the non-condensable gas content, the voids filling up the venturi part of the test section (Figs. 8b and 9b) and might choke the flow. In the experiment, choking conditions are observed in case of sodium cavitation. This choking conditions might be caused the decrease of sound velocity in the liquid due to the increasing amount of cavitation bubbles. These figures also show that the voids (cavity bubbles) are carried away downstream by the flow and collapse (condense) due to the high pressure downstream of the test section.

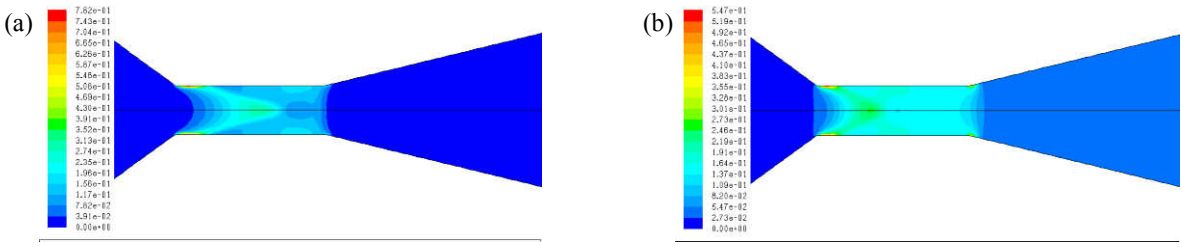

Figure 8. Contours of void fraction in water for K: 0.98 and T: 10.8~13.0°C, a) β : 15 ppm, and b) β : 45 ppm.

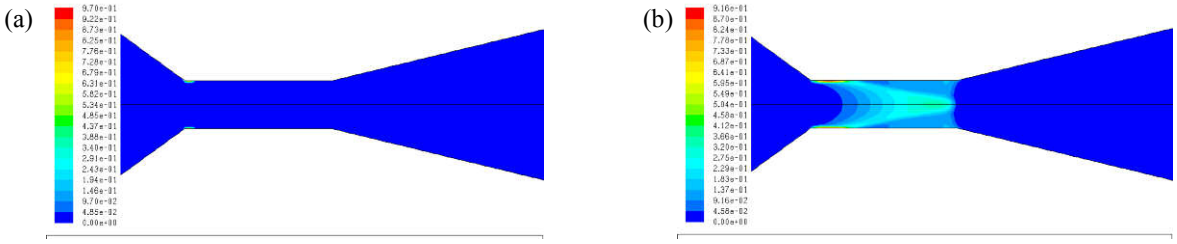

Figure 9. Contours of void fraction in liquid sodium for K: 0.92 and T: 400°C, a) β : 1 ppm, and b) β : 3 ppm.

Parametrical analysis for water and sodium cavitating flows with different non-condensable gas content is shown in Fig. 10. For the same cavitation coefficient value (K=1) and non-condensable gas content (β) for both water and liquid sodium, the void fraction distributions at the venturi region do not show large differences. Increasing the non-condensable gas content (from 10 ppm to 15 ppm) will slightly increase the void fraction close to the inlet and outlet of the venturi since turbulence are enhanced in these parts. The increase are also caused by the increase of the threshold for voids (cavity bubbles) formation in the liquid due to the increase of bubble numbers.

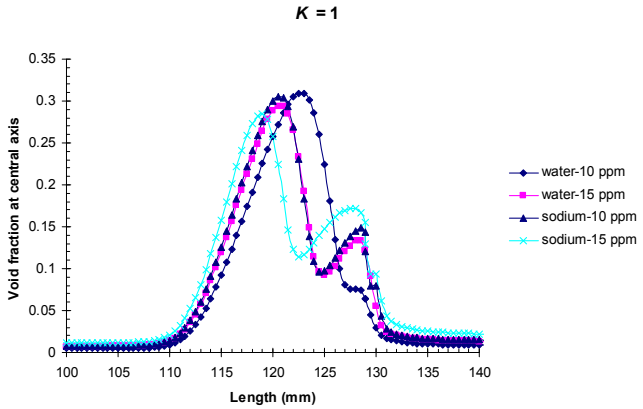

Figure 10. Void fraction distribution for K equals to unity in water and liquid sodium.

8. CONCLUSION

From the numerical simulation of cavitation for water and liquid sodium, it can be concluded that the onset conditions of cavitation are influenced by the amount of non-condensable gases in the liquid. Comparing with the experimental results, the non-condensable gas contents that give close predictions of onset cavitation conditions with the experiments are larger in water than in liquid sodium because of the different solubility of air and argon gas. Parametrical analysis show that the void fractions distribution for water and liquid sodium do not give large differences in case of the same cavitation coefficient and non-condensable gas content.

9. ACKNOWLEDGMENTS

This study is financially sponsored by the Japan Nuclear Energy Safety Organization (JNES).

10. NOMENCLATURE

$\vec{F}$	Body force
h_k	Sensible enthalpy for phase k
K	Cavitation coefficient
k_{eff}	Effective conductivity
n	number of phase
P_{ds}	Downstream static pressure
$Pstag$	Static pressure at stagnant condition (no flow)
P_0	Static pressure at downstream
P_1	Static pressure at venturi part
R_c	Vapor condensation rate
R_e	Vapor generation rate
S_E	External heat source
V_1	Liquid sodium velocity at venturi region
V_0	Liquid sodium velocity at downstream region
β	Non-condensable gas fraction
γ	Effective exchange coefficient
μ_m	Mixture's viscosity
$\vec{\upsilon}_{dr,k}$	Drift velocity for secondary phase k
$\vec{\upsilon}_m$	Mass-averaged velocity
ρ	Liquid sodium density at given temperature
ρ_m	Mixture density
σ	Surface tension

11. REFERENCES

[1] Testud, P., Moussou, P., Hirschberg, A. and Auregan, Y., 2007, "Noise Generated by Single-Hole and Multi-Hole Orifices in A Water Pipe", *Journal of Fluid and Structures* **23**, pp. 163-189.

[2] Koivula, T., 2000, "On Cavitation in Fluid Power", *Proceeding of 1st FPNI-PhD Symposium*, Hamburg, pp. 371-382.

[3] Courbiere, P., 1984, “An acoustic Method for Characterizing the Onset of Cavitation in Nozzles and Pumps”, *International Symposium on Cavitation Inception*, pp. 137-145.
[4] Kale, R. D. and Rajan, M., 2004, “Developments in sodium technology”, *Current Science* **86** (5), pp. 668-675.
[5] Ardiansyah, T., Takahashi, M., Yoshizawa, Y., Nakagawa, M., Miura, K. and Asaba, M., 2008, "Accoustic Noise and Onset of Sodium Cavitation in Venturi", *Proceedings of the 6th Japan-Korea Symposium on Nuclear Thermal Hydraulics and Safety* (in CD), Okinawa, Japan.
[6] Singhal, A. K., Athavale, M. M., Li, H. and Jiang, Y., 2002, "Mathematical Basis and Validation of the Full Cavitation Model", *Journal of Fluids Engineering*, **124**, pp. 617-624.
[7] FLUENT 6.3 User’s Guide, 2006, Fluent Inc.
[8] Fink, J. K., and Leibowitz, L., 1995, “Thermodynamic and Transport Properties of Sodium Liquid and Vapor”. Argonne National Laboratory, USA.
[9] Bistafa, S. R., 1986, “Noise Generated by Cavitation in Orifice-Plates with Some Gaseous Effects”, *International Symposium on Cavitation and Multiphase Flow Noise*, Anaheim, California, pp. 41-52.
[10] Veleckis, E., Dhar, S. K., Cafasso, F. A. and Feder, H. M., 1971, "Solubility of Helium and Argon in Liquid Sodium", *The Journal of Physical Chemistry*, **75**(18), pp. 2832-2838.
[11] Sander, R., 1999, "Compilation of Henry's Law Constants for Inorganic and Organic Species of Potential Importance in Environmental Chemistry", Max-Planck Institute of Chemistry, Germany.